International Journal of Pharmacology

ISSN 1811-7775

science alert

ansinet
Asian Network for Scientific Information

OPEN ACCESS International Journal of Pharmacology

ISSN 1811-7775
DOI: 10.3923/ijp.2025.217.230

Research Article
Mechanistic of Artemisinin Extracts Modulating Cisplatin Resistance in Lung Cancer A549/DDP Cells via the PI3K/Akt Pathway

[1]Weiwei Zeng and [2,3]Lei Xia

[1]Department of Cancer Center, The Second Affiliated Hospital of Chongqing Medical University, Chongqing, 401336, China
[2]Department of Radiation Oncology, Tianjin Medical University Cancer Institute and Hospital, National Clinical Research Center for Cancer, Tianjin's Clinical Research Center for Cancer, Key Laboratory of Cancer Prevention and Therapy, Tianjin, 300060, China
[3]Tianjin Key Laboratory of Radiation Medicine and Molecular Nuclear Medicine, Institute of Radiation Medicine, Chinese Academy of Medical Sciences and Peking Union Medical College, Tianjin, 300110, China

Abstract

Background and Objective: Dihydroartemisinin (DHA) is the principal metabolite of artemisinin, derived from the herb *Artemisia annua* and is known for its efficacy in controlling various forms of malaria and exhibiting enhanced antitumor activity. This work was to demonstrate mechanisms of DHA on proliferation (Pro), apoptosis (Apo) and cisplatin (DDP) resistance in LC A549/DDP cells through PI3K/Akt signaling. **Materials and Methods:** The DHA solid dispersion (DHA-SD) was prepared employing a solvent methodology and its characterization was analyzed. Subsequently, the pharmacokinetic characteristics and bioavailability of DHA-SD were assessed in rats. Human lung adenocarcinoma DDP-resistant cells A549/DDP in the logarithmic growth phase were rolled into Ctrl group, DDP group, DHA group, DHA-SD group, DDP+DHA group and DDP+DHA-SD group. Cell Pro inhibition was measured employing MTT assay, while flow cytometry was employed to assess cell Apo rates. Western blot analysis was performed to evaluate the protein ELs of Caspase-3, Cleaved Caspase-3, Bax, Bcl-2, p-PI3K and p-Akt. **Results:** The DHA-SD possessed similar structures and characteristics to the original DHA. Compared with the Ctrl group, the Pro inhibition rate and Apo rate of the DDP group were significantly increased ($p<0.05$); compared with the DDP group, the Pro inhibition rate and Apo rate were significantly increased and the protein expression of Caspase-3, Cleaved Caspase-3 and Bax were significantly increased and the protein expressions of Bcl-2, p-PI3K and p-Akt were significantly decreased in DHA group, DHA-SD group, DDP+DHA group and DDP+DHA-SD group ($p<0.05$). Among them, the DDP+DHA-SD group had the most obvious changes in cell indexes ($p<0.05$). **Conclusion:** The DHA-SD markedly enhanced the bioavailability of DHA. The combination of DHA and DHA-SD with DDP can inhibit the Pro of LC A549/DDP cells, induce cell Apo and reverse DDP resistance and these effects were associated with the PI3K/Akt signaling.

Key words: Dihydroartemisinin, solid dispersion, bioavailability, LC A549/DDP cells, PI3K/Akt signaling, cisplatin resistance

Citation: Zeng, W. and L. Xia, 2025. Mechanistic of artemisinin extracts modulating cisplatin resistance in lung cancer A549/DDP cells via the PI3K/Akt pathway. Int. J. Pharmacol., 21: 217-230.

Corresponding Author: Lei Xia, Department of Radiation Oncology, Tianjin Medical University Cancer Institute and Hospital, National Clinical Research Center for Cancer, Tianjin's Clinical Research Center for Cancer, Key Laboratory of Cancer Prevention and Therapy, Tianjin, 300060, China

Copyright: © 2025 Weiwei Zeng and Lei Xia. This is an open access article distributed under the terms of the creative commons attribution License, which permits unrestricted use, distribution and reproduction in any medium, provided the original author and source are credited.

Competing Interest: The authors have declared that no competing interest exists.

Data Availability: All relevant data are within the paper and its supporting information files.

INTRODUCTION

Lung cancer (LC), arising from the bronchial mucosa or glandular tissues of the lungs, represents a prevalent malignant tumor contributing to patient mortality. Approximately 80% of LC cases are classified as Non-Small Cell Lung Cancer (NSCLC), with a 5-year survival rate of only 21%[1]. Lung transplantation, chemotherapy and radiation therapy are among the treatment modalities for LC, with chemotherapy being a primary approach. Cisplatin (DDP) serves as a frontline chemotherapeutic agent, but its prolonged usage often leads to drug resistance, resulting in therapy failure[2,3].

Traditional Chinese herbal medicine possesses advantages such as high availability, efficacy and low toxicity. Artemisinin is a sesquiterpene lactone compound with a peroxide bridge, isolated from leaves of *Artemisia annua*, a plant of the Asteraceae family[4]. Dihydroartemisinin (DHA) is a derivative of artemisinin obtained through reduction with sodium borohydride and represents the primary metabolite of artemisinin in the body. The DHA retains the essential antimalarial pharmacophore by converting the C=O group to -OH, thereby greatly enhancing its antimalarial activity[5]. Additionally, DHA exhibits anticancer properties. It engages in multiple mechanisms in the process of cancer suppression, including direct cytotoxicity against tumor cells, induction of cancer cell apoptosis (Apo), inhibition of tumor angiogenesis, suppression of cancer cell metastasis, reversal of multidrug resistance and regulation of the cell cycle[6-10]. Zheng *et al*.[11] demonstrated that DHA can inhibit ovarian cancer cell growth and act as a chemosensitizer to enhance ovarian cancer cell sensitivity to frontline chemotherapy drugs, thereby enhancing treatment efficacy. The DHA suffers from poor water solubility and bioavailability, which limits its clinical adoption. Recently, novel formulations of DHA have been developed using approaches such as liposomes, self-microemulsifying drug delivery systems and self-assembled nanoparticles, which effectively enhance its bioavailability[12-14]. Solid dispersion (SD) is a technique that improves the *in vitro* dissolution of poorly soluble drugs, thereby increasing their bioavailability[15]. By utilizing water-insoluble high molecular weight polymers, enteric materials and lipid-based materials as carriers to prepare sustained-release SDs, the rapid release of drugs can be avoided. Phospholipids possess amphiphilic properties, making them highly effective emulsifiers. As integral components of cell membranes, phospholipids exhibit excellent biocompatibility in the human body. Preparing drug-loaded controlled-release systems using phospholipids as carriers facilitates non-energy-dependent penetration through cell membranes into cells, thereby improving drug bioavailability without inducing cellular toxicity[16]. The DHA demonstrates notable antitumor activity with low toxicity towards normal tissues and cells. Its combination with other antitumor drugs during chemotherapy can enhance its antitumor efficacy without inducing drug resistance. Nevertheless, DHA suffers from poor solution stability.

In this work, phospholipids and other materials were employed as the primary carriers to prepare DHA-SD. The bioavailability of DHA-SD was examined and its effects on proliferation (Pro) and apoptosis (Apo) were investigated in DDP-resistant LC cell line A549/DDP. Additionally, the underlying mechanism involving PI3K/Akt signaling was examined, to provide a theoretical basis for reversing DDP resistance in LC cells and enhancing the therapeutic efficacy against DDP-resistant LC.

MATERIALS AND METHODS

Study area: This work was conducted in The Second Affiliated Hospital of Chongqing Medical University from May, 2022 to August, 2023.

Fabrication of SD of DHA: The DHA (purity $\geq$98%, Shanghai Fortune bio-tech Biotechnology Co., Ltd., China) was taken and DHA-SD was prepared employing a solvent method[17]. According to the procedure, DHA, H-β-cyclodextrin (H-β-CD), soybean phospholipids, citric acid and other excipients were sequentially weighed and placed in a 100% ethanol solution. They were stirred using an OS-Pro magnetic stirrer (Shanghai Kexing Instrument Co., Ltd., China) at 40°C until fully dissolved, followed by continuous stirring for 20 min. The solution was then subjected to a vacuum rotary evaporator (Zhengzhou Keda Machinery Instrument Equipment, China) at 50°C to remove the 100% ethanol. Subsequently, the residual 100% ethanol was removed by vacuum drying. After grinding and passing through a 60-mesh sieve, the final DHA-SD material was obtained.

Characterization of SD of DHA: (1) The XRD-6100 X-ray Diffraction Analyzer (Shanghai Wak Instrument Co., Ltd., China) was employed to analyze the raw material DHA and DHA-SD with a voltage of 40 kV, current of 40 mA and scan speed of 10°/min over the 2θ range of 3~4°. (2) A small amount of raw material DHA and DHA-SD was applied to conductive adhesive and subjected to gold sputtering and a Gemini SEM 500 scanning electron microscope (Zeiss, USA) was used to observe the morphology of each sample. (3) For each sample, 2 mg of raw material DHA and DHA-SD were placed in sealed aluminum pans. The glass transition

temperature (Tg) of each sample was determined employing DSC-600 Differential Scanning Calorimeter (Wuxi DEANS Instrument Technology Co., Ltd., China) with a heating rate of 10°C/min, nitrogen flow rate of 40 mL/min and heating range of 30~300°C, to evaluate their thermal properties. (4) Appropriate amounts of raw material DHA and DHA-SD were mixed with dried KBr, ground and pressed into pellets. The LIDA-22 Fourier Transform Infrared Spectrometer (Tianjin Hengchuang Lida Technology Co., Ltd., China) was used in the range of 4,000~400 cm^{-1} to analyze the chemical bonds, functional groups and changes in the crystal structure of each sample.

Bioavailability of DHA-SD: Twelve healthy male SD rats (2~2.5 months old, weighing 350~380 g; Yunnan Luoyu Biotechnology Co., Ltd., China) were randomly and equally rolled into DHA and DHA-SD groups. Before drug administration, all rats fasted for 12 hrs but had free access to water. The DHA group received an oral suspension of raw material DHA at a dose of 0.5 mL/kg, while the DHA-SD group received an oral suspension of DHA-SD at the same dose. Blood samples of 0.25 mL were collected via jugular vein catheter at 0.25, 0.5, 1, 3, 6, 12 and 24 hrs after drug administration. The collected blood was anticoagulated and centrifuged and the supernatant was separated. The 50 µL of plasma was mixed with 5 µL of 10% formic acid and 5 µL of 30% hydrogen peroxide, followed by the addition of 50 µL of the internal standard DHA-acetonitrile working solution (100 ng/mL) and 150 µL of acetonitrile working solution. After vortex mixing, the sample was centrifuged at 12,000 rpm/min at 4°C for 10 min. A 100 µL aliquot was taken and centrifuged in an inner insert at 12,000 rpm/min at 4°C for 5 min and 20 µL was injected for LC-MS/MS quantitative analysis. The chromatographic column used was Zorbax Eclispe C18, with dimensions of 50×4.5 mm, operating at 30°C and a flow rate of 0.5 mL/min. Total run time was 6.5 min, with mobile phase A consisting of a 10 mmol/L ammonium acetate-5% methanol solution and mobile phase B consisting of a 50% methanol-acetonitrile solution. Blood concentration-time curves were plotted and AUC was calculated. The elimination half-life, peak drug concentration (C_{max}) and time to reach peak concentration (T_{max}) were determined by adopting the Best Fit method. The bioavailability was calculated based on $AUC_{0\sim t}$. All experiments were approved by Ethics Committee of Hospital and in accordance with the Guide for the Care and Use of Laboratory Animals published by the United States National Institutes of Health.

Cell grouping and treatment: The A549/DDP cells (Aoruisai Biological Cell Bank, China) were seeded in DMEM (+10% FBS and 1% penicillin-streptomycin). Culture was maintained in a carbon dioxide-saturated humidified incubator at 37°C. When cell confluence reached 80%, they were passaged after digestion with 0.25% trypsin. The cells were then assigned into Ctrl, DDP, DHA, DHA-SD, DDP+DHA and DDP+DHA-SD groups. In Ctrl group, cells were cultured normally with no drug treatment. The DDP, DHA, DHA-SD, DDP+DHA and DDP+DHA-SD groups were treated with a culture medium containing 25 µmol/L DDP (Sigma-Aldrich, USA), 250 µmol/L DHA, 250 µmol/L DHA-SD, 25 µmol/L DDP+250 µmol/L DHA and 25 µmol/L DDP+250 µmol/L DHA-SD, respectively.

Cell Pro activity detected by MTT assay: Firstly, influences of various concentrations of DHA and DHA-SD on the Pro viability of A549 cells (Aoruisai Biological Cell Bank, China) and A549/DDP cells were evaluated. A total of 5×10^5 cells in logarithmic growth phase (LGP) were seeded into 96-well plates and applied with culture media containing 0, 25, 50, 100, 150, 200, 250 and 300 µmol/L concentrations of DHA or DHA-SD, respectively. According to the instructions of the Methylthiazolyldiphenyl tetrazolium bromide (MTT) detection kit (Sigma-Aldrich, USA), after 48 hrs of routine incubation, 20 µL of 50 mg/mL MTT reagent was applied and plates were further incubated for 4 hrs followed by centrifugation for 10 min. The supernatant was discarded and 150 µL of dimethyl sulfoxide (DMSO, Sigma-Aldrich, USA) was applied to each well, followed by shaking to ensure homogeneity. The absorbance (A value) was measured at 490 nm employing an HBS-1096A ELISA reader (Nanjing Detie Experimental Equipment Co., Ltd., China) and cell Pro inhibition rate was calculated. Each experiment was repeated thrice.

Secondly, A549/DDP cells in LGP were seeded into 96-well plates at 5×10^5 cells/well. Following the grouping treatment method mentioned in Section 2.4, the cells were treated with drug-containing culture media. After 48 hrs of drug exposure, the cell Pro-inhibition rate of each group was assessed by employing an MTT assay. Each experiment was repeated thrice.

Apo detected by FCM: The A549/DDP cells in LGP were seeded into 96-well plates at 5×10^5 cells/well and treated with drug-containing culture media according to the grouping methodology described in Section 2.4. After 48 hrs of drug exposure, cells from each group were collected. According to the instructions of the Annexin V-Fluorescein Isothiocyanate (FITC)/Propidium Iodide (PI) kit (Sigma-Aldrich, USA), phosphate-buffered saline (PBS) was utilized twice for cell washing and then 100 µL of 1×Binding buffer was applied to each well. Subsequently, 10 µL of FITC-labeled Annexin V

working solution and 5 µL of PI working solution were utilized and the plate was incubated in the dark for 15 min. Afterward, 300 µL of 1×Binding buffer was applied and the cell Apo rate was analyzed employing CytoFLEX flow cytometry (Beckman Kurt, USA). Each experiment was repeated thrice.

Western blot (WB): The A549/DDP cells in LGP were seeded into 96-well plates at 5×10^5 cells/well and treated with drug-containing culture media according to the grouping methodology described in Section 2.4. After 48 hrs of drug exposure, cells from each group were collected. Total protein extraction was implemented using Radioimmunoprecipitation Assay lysis buffer (Beijing Solarbio Technology Co., Ltd., China) and protein quantification was performed employing Bicinchoninic acid Protein Quantitative kit (Shanghai Beyotime Biotechnology Co., Ltd., China). The SDS-PAGE was employed to separate proteins, then transferred onto PVDF membrane, followed by room temperature blocking. Subsequently, membrane was incubated with primary antibodies against Caspase-3, Cleaved Caspase-3, Bax, Bcl-2, PI3K, p-PI3K, Akt, p-Akt and GAPDH (diluted 1:2,000; Abcam; UK) and incubated overnight at 4°C. After PBS washing, the membrane was incubated with horseradish peroxidase-conjugated secondary antibody (diluted 1:5,000; Abcam; UK) at 25°C in the dark for 2 hrs. Protein bands were visualized employing an enhanced chemiluminescence detection kit (Shanghai Beyotime Biotechnology Co., Ltd., China) and the gel images were scanned employing WD-9413A gel imager (Beijing Liuyi Instrument Co., Ltd., China). The ImageJ was employed for the analysis of relative band intensities of the target proteins.

Statistical analysis: Employing SPSS 22.0, all data were denoted as Mean±Standard Deviation ($\bar{x}\pm s$). One-way analysis of variance was adopted for comparisons among multiple groups and pairwise comparisons were conducted employing the LSD-t test. The $p<0.05$ was statistically significant.

RESULTS

Characterization and analysis of DHA-SD: The XRD was adopted for the crystal phase analysis of the raw material DHA and DHA-SD. In Fig. 1, the raw material DHA exhibited distinct characteristic diffraction peaks and similar characteristic diffraction peaks were also present in DHA-SD.

The surface morphology of the raw material DHA and DHA-SD was observed employing SEM. In Fig. 2, the raw material DHA exhibited needle-like crystals, while DHA-SD forms block-like and relatively uniform particles after aggregation with the carrier material. The DHA-SD underwent a noticeable change in morphology.

In Fig. 3a, the raw material DHA exhibited a distinct melting point peak at around 262°C, which serves as an indicator of DHA crystallinity. In contrast, no characteristic peak of DHA was detected in DHA-SD, possibly due to the dispersion of DHA within the SD. Subsequently, FTIR was employed to analyze chemical bonds, functional groups and crystal structure changes of the raw material DHA and DHA-SD. In Fig. 3b, the raw material DHA exhibits stretching vibrations of O-H at 3,409 cm^{-1}, those of C-O aldehyde at 1,162 and 1,095 cm^{-1}, those of O-O at 825 cm^{-1} and bending vibrations of O-O-C at 878 cm^{-1}. Similarly, DHA-SD also showed characteristic peaks at 3,408 cm^{-1} for semi-aldehyde O-H stretching vibration and other peaks similar to those of the raw material DHA.

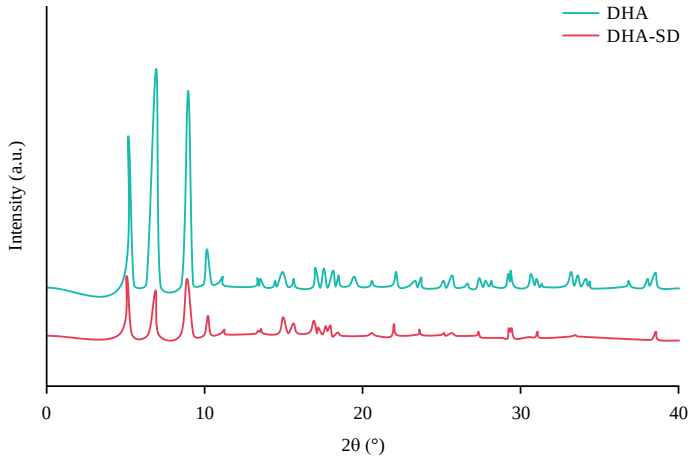

Fig. 1: XRD patterns of DHA and DHA-SD

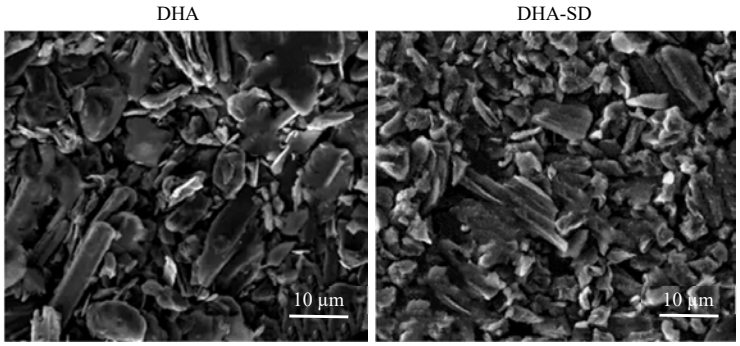

Fig. 2: SEM observation of DHA and DHA-SD

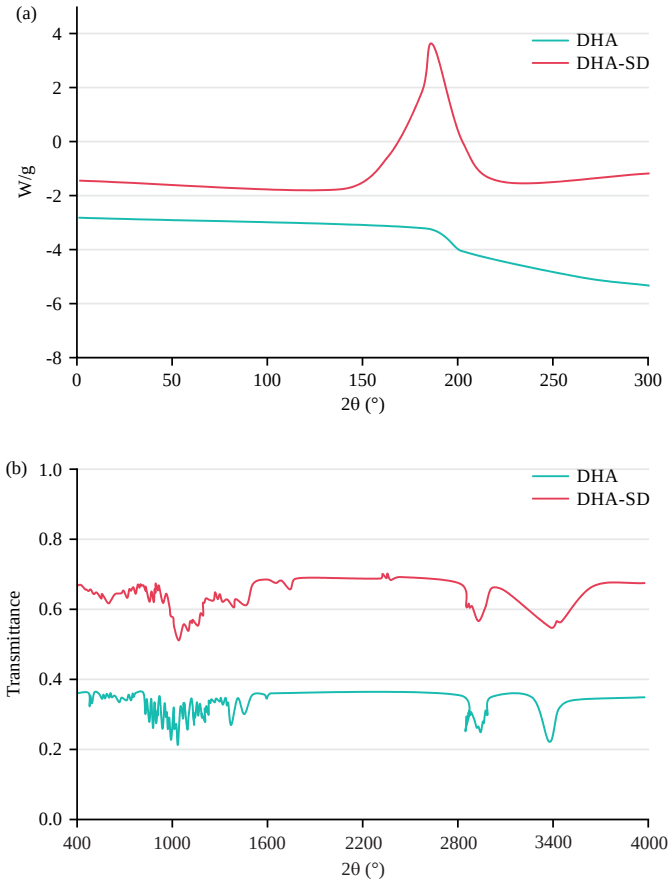

Fig. 3(a-b): DSC and FTIR spectra of DHA and DHA-SD, (a) DSC curve and (b) FTIR spectrum

Bioavailability analysis of DHA-SD: The raw material DHA and DHA-SD suspension formulations were injected into SD rats and blood concentration-time curves were plotted for the analysis of their pharmacokinetics. Hence, AUC of blood concentration-time curve is an imperative parameter for evaluating the bioavailability and bioequivalence of the formulations. In Fig. 4, the raw material DHA reached its peak concentration in the plasma at 0.25 hrs and then the blood drug concentration gradually decreased. After preparing DHA-SD, the drug exposure of DHA also peaked at 0.25 hrs and its exposure was remarkably superior to that of the raw material DHA.

After intravenous injection of the raw material DHA and DHA-SD suspension formulations, blood concentration-time curves were plotted to detect the values of C_{max}, T_{max} and $AUC_{0\sim t}$. The C_{max}, T_{max} and AUC are crucial pharmacokinetic

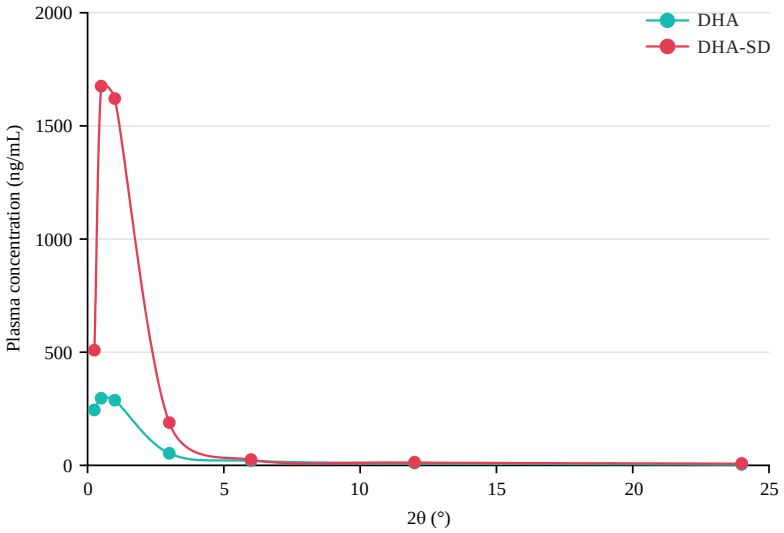

Fig. 4: Plasma concentration-time curves of DHA and DHA-SD *in vivo*

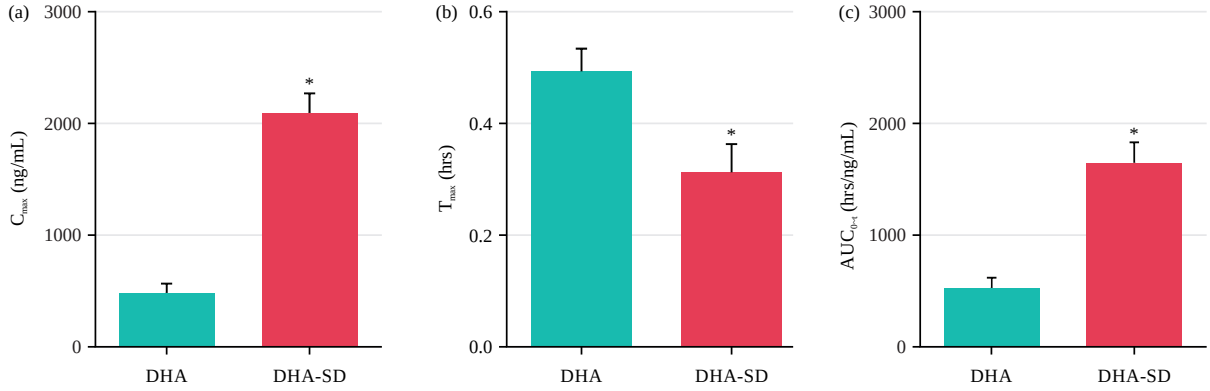

Fig. 5(a-c): Parameters of plasma concentration-time curve of DHA and DHA-SD *in vivo*, (a) Peak concentration of drugs, (b) Peak time of drug concentration and (c) AUC of plasma concentration-time curve
*p<0.05 vs DHA group

parameters. In Fig. 5(a-c), the C_{max} and AUC_{0-t} values of DHA-SD were remarkably superior to those of DHA ($p<0.05$), while the T_{max} value of DHA-SD was greatly inferior to that of DHA ($p<0.05$).

Effects of DHA on Pro of A549 and A549/DDP cells: In Fig. 6 (Fig. 6a: A549, Fig. 6b: A549/DDP), with the increasing concentrations of raw material DHA and DHA-SD, the Pro of both A549 and A549/DDP cells decreased markedly. Moreover, at concentrations of 150, 200, 250 and 300 µmol/L, DHA-SD exhibited markedly greater inhibition of Pro in A549 and A549/DDP cells relative to DHA ($p<0.05$).

Effect of DHA on Pro of A549/DDP cells: Differences in Pro activity among A549/DDP cell groups were assessed. In Fig. 7, cell Pro inhibition rates substantially increased in all treatment groups versus Ctrl ($p<0.05$). Relative to DDP group, negligible difference existed in cell Pro inhibition rate in DHA group ($p>0.05$), while DHA-SD, DDP+DHA and DDP+DHA-SD groups exhibited substantially increased cell Pro inhibition rates ($p<0.05$). The DDP+DHA group and DDP+DHA-SD group showed substantially increased cell Pro inhibition rates versus DHA-SD group ($p<0.05$). Moreover, DDP+DHA-SD group exhibited a markedly higher cell Pro inhibition rate than DDP+DHA group ($p<0.05$).

Effect of DHA on Apo of A549/DDP cells: In this work, FCM was employed to detect differences in Apo rates among various A549/DDP cell groups. In Fig. 8(a-b), relative to Ctrl group, cell Apo rates substantially increased in all treatment

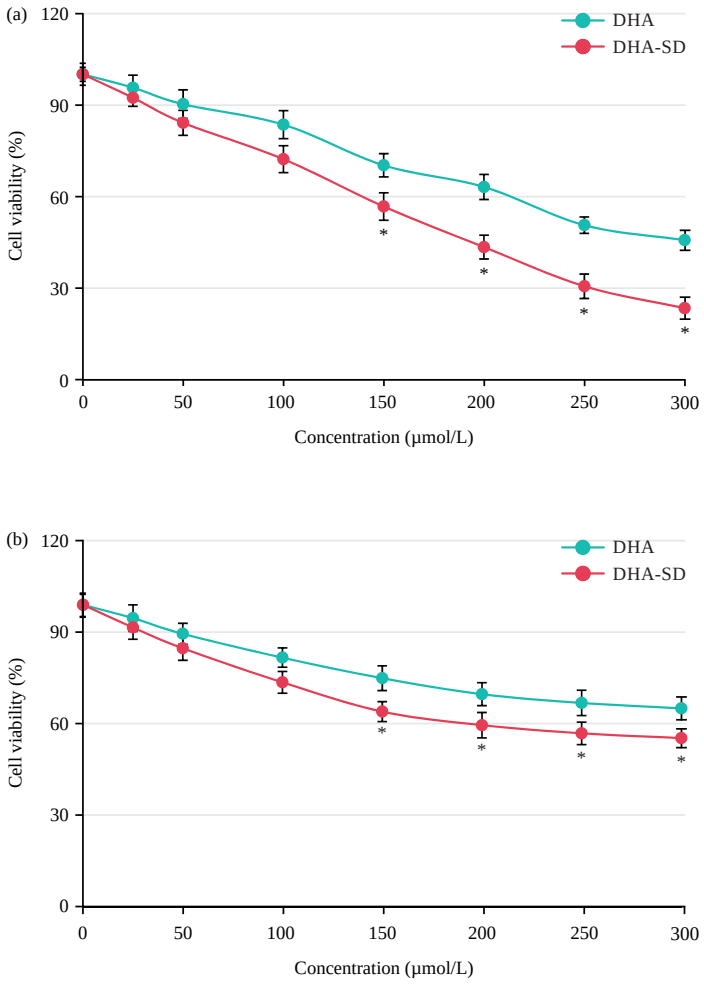

Fig. 6(a-b): Effects of DHA and DHA-SD on Pro of NSCLC cells, (a) Pro activity of A549 cells and (b) Pro activity of A549/DDP cells

*p<0.05 vs DHA group

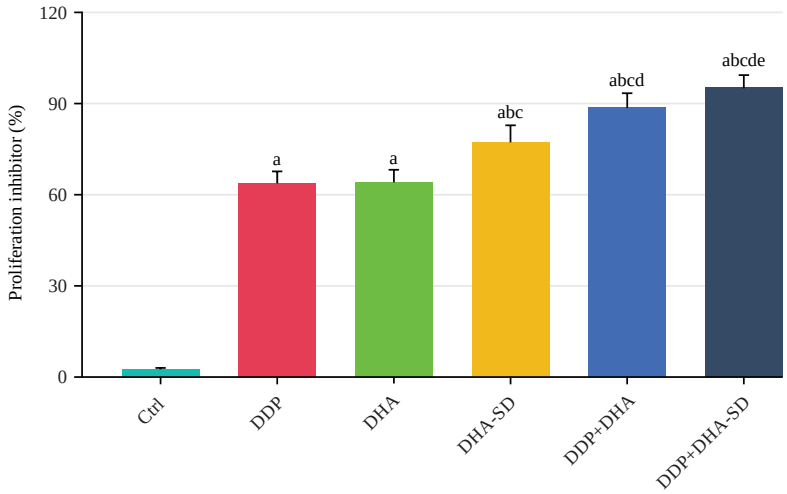

Fig. 7: Comparison of Pro inhibition rate of A549/DDP cells

[a]p<0.05 vs Ctrl group, [b]p<0.05 vs DDP group, [c]p<0.05 vs DHA group, [d]p<0.05 vs DHA-SD group and [e]p<0.05 vs DDP+DHA group

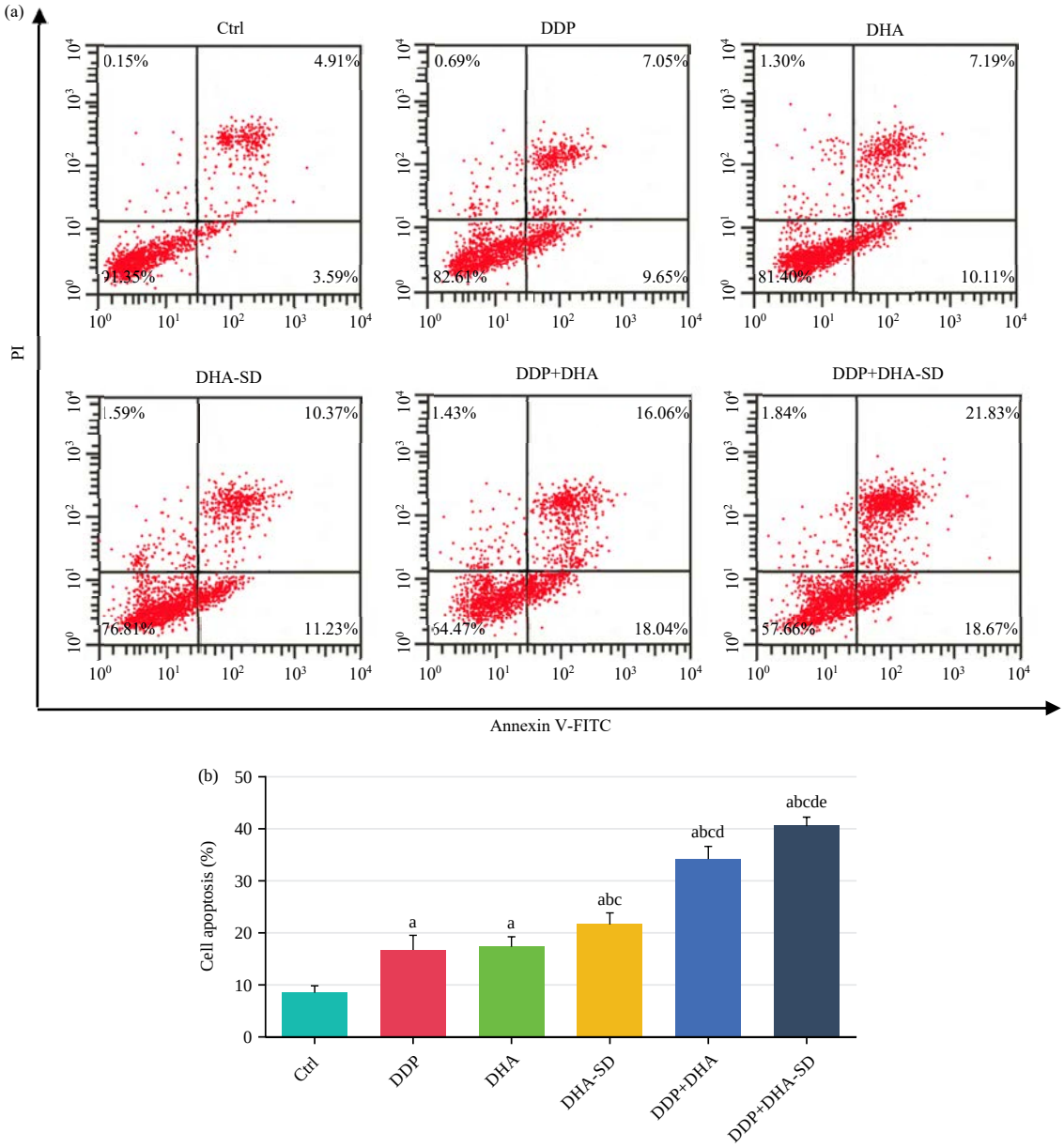

Fig. 8(a-b): Comparison of Pro inhibition rate of A549/DDP cells, (a) FCM and (b) Apo rate

[a]p<0.05 vs Ctrl group, [b]p<0.05 vs DDP group, [c]p<0.05 vs DHA group, [d]p<0.05 vs DHA-SD group and [e]p<0.05 vs DDP+DHA group

groups (p<0.05). Neglectable differences existed in cell Apo rate in DHA group versus DDP group (p>0.05), while DHA-SD, DDP+DHA and DDP+DHA-SD groups exhibited substantially increased cell Apo rates (p<0.05). The DDP+DHA group and DDP+DHA-SD group showed substantially increased cell Apo rates versus DHA-SD group (p<0.05). Moreover, relative to DDP+DHA group, DDP+DHA-SD group exhibited a markedly higher cell Apo rate (p<0.05).

The differences in the ELs of Apo-related proteins in various A549/DDP cell groups were detected. In Fig. 9 (Fig. 9a: Western blotting result and Fig. 9(b-e): Comparison of the relative expression levels of each protein), relative to Ctrl group, the ELs of Caspase-3, Cleaved Caspase-3 and Bax proteins substantially increased, while Bcl-2 protein EL dramatically decreased in all treatment groups (p<0.05). Neglectable difference existed in the expression of Caspase-3, Cleaved Caspase-3, Bax and Bcl-2 proteins between DDP and DHA group (p>0.05), while DHA-SD group, DDP+DHA group and DDP+DHA-SD group showed substantially increased ELs of Caspase-3, Cleaved Caspase-3 and Bax proteins, along with

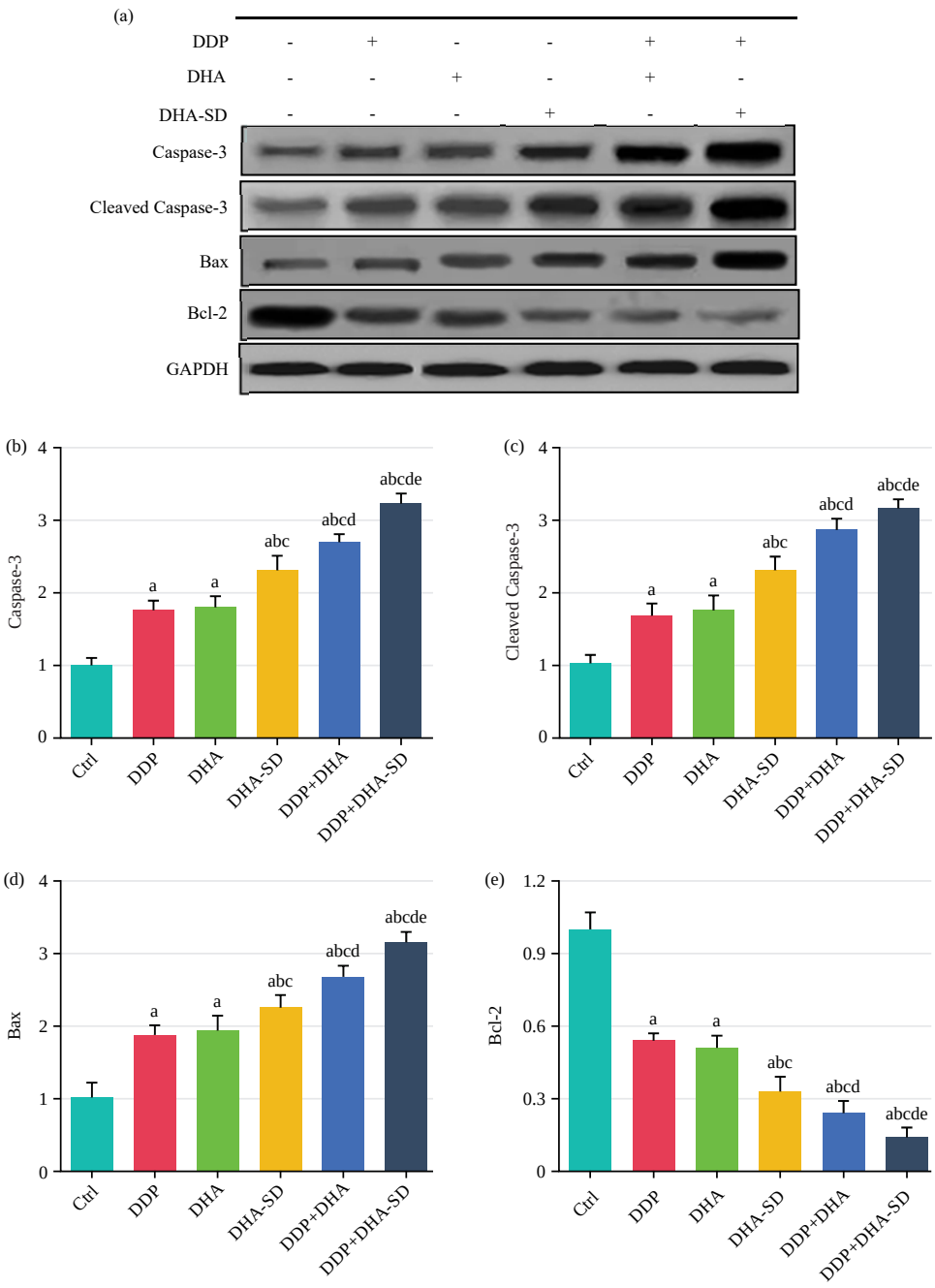

Fig. 9(a-e): Comparison of Apo-related protein ELs in A549/DDP cells, (a) WB, (b) Relative EL of Caspase-3 protein, (c) Relative EL of Cleaved Caspase-3 protein, (d) Relative EL of Bax protein and (e) Relative EL of Bcl-2 protein

[a]p<0.05 vs Ctrl group, [b]p<0.05 vs DDP group, [c]p<0.05 vs DHA group, [d]p<0.05 vs DHA-SD group and [e]p<0.05 vs DDP+DHA group

a notable decrease in Bcl-2 protein EL ($p<0.05$). Additionally, when compared to the DHA-SD group, the DDP+DHA group and DDP+DHA-SD group exhibited substantially increased ELs of Caspase-3, Cleaved Caspase-3 and Bax proteins, while Bcl-2 protein EL was dramatically decreased ($p<0.05$). The DDP+DHA-SD group exhibited substantially increased ELs of Caspase-3, Cleaved Caspase-3 and Bax proteins than DDP+DHA group, while Bcl-2 protein EL was dramatically decreased ($p<0.05$).

Influence of DHA on the ELs of PI3K/Akt pathway-related proteins in A549/DDP cells: In this work, WB was performed to assess the differences in the ELs of PI3K/Akt pathway-related proteins among different groups of A549/DDP

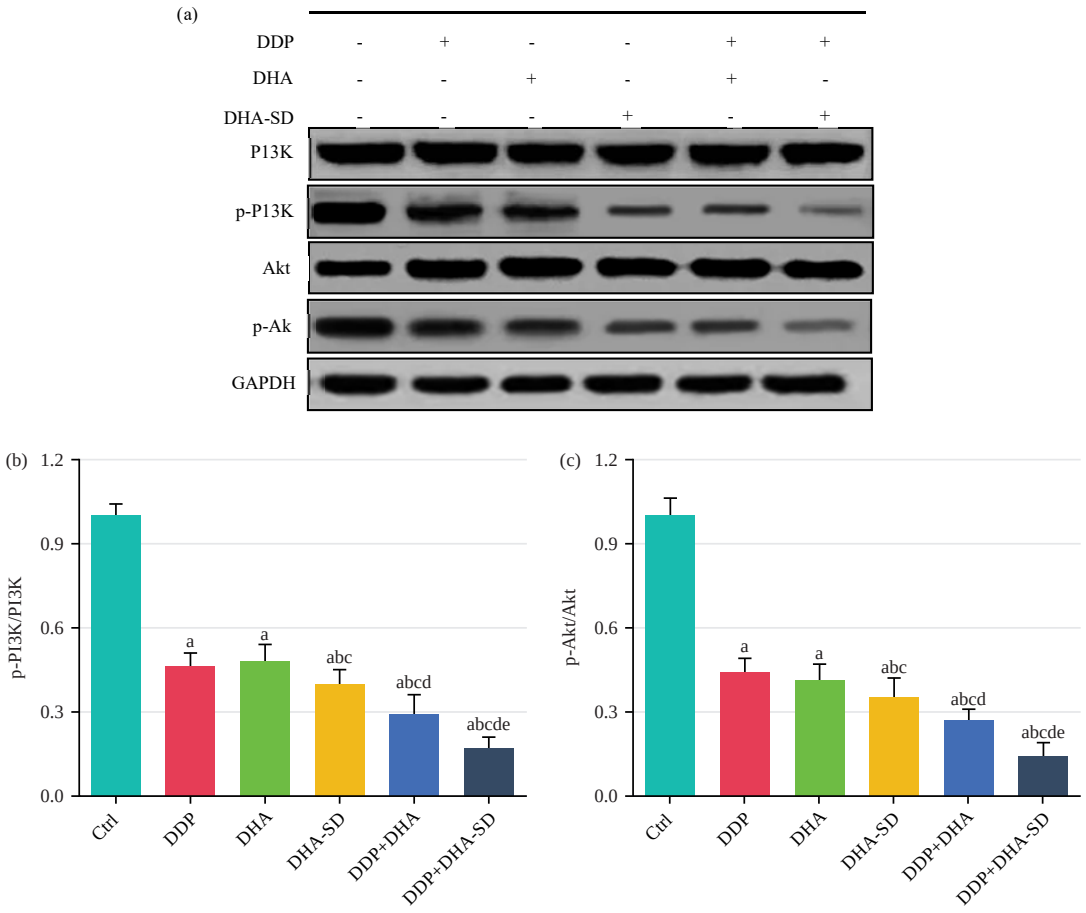

Fig. 10(a-c): Comparison of PI3K/Akt pathway-related proteins ELs in A549/DDP cells, (a) WB, (b) Relative EL of p-PI3K/PI3K protein and (c) Relative EL of p-Akt/Akt protein

[a]p<0.05 vs Ctrl group, [b]p<0.05 vs DDP group, [c]p<0.05 vs DHA group, [d]p<0.05 vs DHA-SD group and [e]p<0.05 vs DDP+DHA group

cells. In Fig. 10 (Fig. 10a: Western blotting result, Fig. 10(b-c): Comparison of the relative expression levels of each protein), ELs of p-PI3K/PI3K and p-Akt/Akt proteins were dramatically decreased in all treatment groups versus Ctrl group ($p<0.05$). Moreover, a neglectable difference existed in the p-PI3K/PI3K and p-Akt/Akt protein ELs in DHA group when compared to DDP group ($p>0.05$), while DHA-SD group, DDP+DHA group and DDP+DHA-SD group showed dramatically decreased ELs of p-PI3K/PI3K and p-Akt/Akt proteins ($p<0.05$). Relative to DHA-SD group, ELs of p-PI3K/PI3K and p-Akt/Akt proteins were dramatically decreased in DDP+DHA group and DDP+DHA-SD group ($p<0.05$). The DDP+DHA-SD group exhibited dramatically decreased ELs of p-PI3K/PI3K and p-Akt/Akt proteins versus DDP+DHA group ($p<0.05$).

DISCUSSION

In this work, DHA-SD composite materials were prepared and characterized. The XRD was employed for identifying substances in their amorphous and crystalline states, where peaks in the spectrum corresponded to crystalline substances (sharp peaks) and amorphous substances (broad peaks)[18]. In the XRD spectrum, the peak area represents the crystalline content, with larger areas indicating higher crystalline phase content; narrower peaks indicate larger crystal grain size[19]. This work found that the characteristic diffraction peaks in the XRD spectra of DHA-SD and raw material DHA were similar, indicating that DHA in the prepared DHA-SD remained in crystalline form. Subsequently, morphological observations of DHA-SD were conducted. The SEM is an observation technique positioned between transmission electron microscopy and optical microscopy, which utilizes a narrow, focused, high-energy electron beam to scan samples. By interacting with the substance, the electron beam stimulates various physical interactions, allowing for the collection, magnification and re-imaging of these interactions to achieve microstructural characterization of the material[20]. This work revealed that raw material DHA exhibited needle-like crystals,

while DHA-SD appeared as homogeneous block-shaped particles. The differing morphological structures of DHA and DHA-SD may be attributed to interactions between the drug and polymer, resulting in changes in the material's physical form[21]. The DSC is a thermal analysis technique that measures the power difference between a sample and a reference material under controlled temperature programming, revealing their relationship with temperature[22]. The FTIR spectra arise from molecular vibrations and rotational transitions, wherein atoms within chemical bonds or functional groups continuously vibrate (or rotate), with their vibration frequency corresponding to the infrared light's frequency[23]. When molecules are exposed to infrared light, chemical bonds or functional groups within the molecules can absorb energy through vibration, with different bonds or groups exhibiting distinct absorption frequencies that appear at specific positions in the infrared spectrum, providing information about the chemical bonds or functional groups present in the molecule[24]. Essentially, FTIR is a method used to determine molecular structures and identify compounds based on relative atomic vibrations and molecular rotation. Subsequently, DSC and FTIR techniques were employed for the characteristic analysis of DHA-SD, confirming the successful preparation of DHA-SD material and demonstrating strong interactions between DHA and excipients.

Subsequently, this work evaluated the bioavailability of DHA-SD. The blood concentration-time curve is directly proportional to the total drug absorption, reflecting the extent of drug absorption[25]. Therefore, the area under the blood concentration-time curve (AUC) is an important parameter for assessing formulation bioavailability and bioequivalence. The C_{max} and T_{max} are important pharmacokinetic parameters, which reflect the maximum concentration and time that the drug can reach in the blood after entering the body, respectively[26]. A larger AUC indicates more complete drug absorption by the organism from the formulation[27]. This work found that after administration of DHA-SD, the C_{max} and AUC_{0-t} values were significantly higher than those of DHA, while T_{max} was notably shorter than that of DHA. This suggests a significant improvement in the bioavailability of DHA after preparing DHA-SD, thereby enhancing drug absorption *in vivo*.

The DDP is an important strategy for reducing the risk of recurrence in advanced LC and after surgical resection[28]. However, prolonged use of DDP can lead to acquired drug resistance in patients, thereby impacting its efficacy in treating NSCLC. Mechanisms contributing to DDP resistance include reduced intracellular accumulation, increased efflux, enhanced DNA repair capacity and Apo suppression[29]. The DHA is a significant derivative of artemisinin, known not only for its anti-malarial activity but also exhibiting anticancer effects three times greater than its antimalarial activity[30]. This work observed that Pro viability of A549 and A549/DDP cells significantly decreased after treatment with DHA and DHA-SD, with DHA-SD demonstrating notably lower cell Pro activity compared to DHA. Phospholipids are amphiphilic molecules capable of enhancing the dissolution potential of poorly soluble drugs. The H-β-CD can encapsulate drugs within its hydrophobic cavity, acting as a complexing agent to improve drug solubility and bioavailability[31]. Furthermore, this work found that the Pro activity of A549/DDP cells was significantly lower after treatment with DDP+DHA and DDP+DHA-SD compared to treatment with DHA alone or DHA-SD alone, with the highest cell Pro inhibition observed after DDP+DHA-SD treatment. The DDP is a foundational chemotherapy drug for LC treatment and DDP resistance is a major factor leading to lower survival rates and poor prognosis in patients[32]. Artemisinin is a safe and effective antimalarial drug derived from the medicinal herb *Artemisia annua*. The DHA is the principal metabolite of artemisinin in the body, exhibiting better water solubility and antimalarial efficacy compared to artemisinin. Artemisinin contains a unique peroxide bridge that, upon reaction with ferrous ions, generates oxygen free radicals, inducing molecular damage and cell death or directly damaging cell structures and functions through oxidative mechanisms, ultimately leading to cell death[33]. Therefore, the preparation of DHA-SD formulation enhances DHA solubility, improves bioavailability and consequently more effectively inhibits Pro of A549/DDP cells, exhibiting a favorable role in reversing drug resistance in tumor cells.

Cell Apo refers to the orderly and autonomous death process regulated by genes during development in most cells within an organism, while Apo of tumor cells involves various cellular molecules and pathophysiological processes[34,35]. The Apo is a programmed cell death mechanism crucial for maintaining normal organism development and tissue homeostasis. Malignant tumor cells require substantial ferrous ions for synthesizing deoxyribonucleic acid precursors and the cytotoxic effects mediated by iron-generated radicals in DHA can act on target cells correlating positively with intracellular iron content[36]. Furthermore, this work observed that the Apo rate of A549/DDP cells was significantly higher after treatment with DDP+DHA and DDP+DHA-SD compared to treatment with DHA alone or DHA-SD alone, with the highest Apo rate observed after DDP+DHA-SD treatment. When DHA is used for tumor treatment, its combination with iron chelators or induction of transferrin receptor expression can greatly increase intracellular ferrous ion content in tumor cells,

thereby directly enhancing the cytotoxic effects of the drug against resistant tumor cells[37]. Subsequently, this work investigated changes in the expression levels of Apo-related proteins in cells. The Bax and Bcl-2 are members of the Bax family of homologous proteins and previous research has established a close relationship between the expression levels of Bcl-2-related proteins and DDP resistance[38]. Furthermore, this work found that after treatment with DDP+DHA and DDP+DHA-SD, the expression levels of Apo-related proteins Caspase-3, Cleaved Caspase-3 and Bax in A549/DDP cells were significantly higher compared to treatment with DHA alone or DHA-SD alone, with the highest protein expression levels observed after DDP+DHA-SD treatment. Tang *et al*.[39] demonstrated that DHA combined with DDP induced significant upregulation of Caspase-3 expression levels in endometrial and cervical cancer cells, showing dose and time dependency. The Bcl-2 is an anti-apoptotic factor, while Caspase-3 is a pro-apoptotic factor, both of which play a role in the process of cell Apo[40]. This work indicates that DHA-SD can promote the expression of pro-apoptotic proteins Caspase-3, Cleaved Caspase-3 and Bax, while inhibiting the expression of Bcl-2 protein, thereby promoting Apo of A549/DDP cells and contributing to reversal of drug resistance.

The DHA is a semi-synthetic derivative of artemisinin, widely used in the treatment of malaria. In recent years, studies have discovered that DHA also exhibits antitumor activity, capable of inhibiting tumor cell Pro and inducing Apo through various mechanisms[41]. The PI3K/Akt signaling pathway is an important cellular signaling pathway involved in regulating processes such as cell survival, Pro and Apo. Upon activation of PI3K, Phosphatidylinositol 4,5-Bisphosphate (PIP2) is produced, which then converts to phosphatidylinositol 3,4,5-trisphosphate (PIP3) by activating Akt protein kinase[42]. The PIP3 further activates downstream signaling molecules, promoting cell Pro and inhibiting Apo. However, excessive activation of the PI3K/Akt signaling pathway can lead to abnormal Pro of tumor cells and enhanced resistance to Apo[43].

This work found that the phosphorylation levels of Apo-related proteins PI3K and Akt were significantly lower in A549/DDP cells after treatment with DDP+DHA and DDP+DHA-SD compared to treatment with DHA alone or DHA-SD alone, with the lowest phosphorylation levels observed after DDP+DHA-SD treatment. These results indicate that DHA-SD can inhibit the activation of the PI3K/Akt signaling pathway to suppress Pro and promote Apo of A549/DDP cells. Additionally, DHA may exert its antitumor effects through other mechanisms. Studies have shown that DHA can inhibit the angiogenic capacity of tumor cells, reducing tumor blood supply and thereby inhibiting tumor growth and metastasis[44]. The DHA can also inhibit the migration and invasion capabilities of tumor cells, thereby suppressing tumor metastasis and invasion[45]. These mechanisms are likely closely associated with the antitumor effects of DHA.

CONCLUSION

The DHA solid dispersion (DHA-SD) exhibited improved solubility and higher bioavailability. Moreover, DHA-SD effectively suppressed the Pro of LC A549/DDP cells, reversed their resistance to DDP and may be associated with inhibition of PI3K/Akt signaling to promote Apo. Nevertheless, the current research still has certain limitations and shortcomings that require further investigation to address. Future studies need to explore how DHA selectively inhibits tumor cell Pro and promotes Apo while investigating potential toxicity in normal cells. In summary, the findings of this work are of notable importance for a deeper understanding of the antitumor mechanisms of DHA and the development of DHA formulations. Further research will shed light on the selective actions of DHA against tumor cells and its potential as a therapeutic agent, making a valuable contribution to the field of cancer research and drug development.

SIGNIFICANCE STATEMENT

To reverse the drug resistance of cisplatin resistant strains of lung cancer, dihydroartemisinin was extracted from *Artemisia annua* and prepared to solid dispersion, which combined with cisplatin could inhibit the proliferation of A549/DDP cells and reverse cisplatin resistance. The results are of great significance for finding new drugs to improve the therapeutic effect of cisplatin resistance in lung cancer.

REFERENCES

1. Duma, N., R. Santana-Davila and J.R. Molina, 2019. Non-small cell lung cancer: Epidemiology, screening, diagnosis, and treatment. Mayo Clin. Proc., 94: 1623-1640.
2. Konoshenko, M., Y. Lansukhay, S. Krasilnikov and P. Laktionov, 2022. MicroRNAs as predictors of lung-cancer resistance and sensitivity to cisplatin. Int. J. Mol. Sci., Vol. 23. 10.3390/ijms23147594.
3. Ashrafizadeh, M., A. Zarrabi, K. Hushmandi, F. Hashemi and E.R. Moghadam *et al*., 2021. Lung cancer cells and their sensitivity/resistance to cisplatin chemotherapy: Role of microRNAs and upstream mediators. Cell. Signalling, Vol. 78. 10.1016/j.cellsig.2020.109871.

4. Talman, A.M., J. Clain, R. Duval, R. Ménard and F. Ariey, 2019. Artemisinin bioactivity and resistance in malaria parasites. Trends Parasitol., 35: 953-963.
5. Dai, X., X. Zhang, W. Chen, Y. Chen, Q. Zhang, S. Mo and J. Lu, 2021. Dihydroartemisinin: A potential natural anticancer drug. Int. J. Biol. Sci., 17: 603-622.
6. Bai, B., F. Wu, K. Ying, Y. Xu and L. Shan *et al*., 2021. Therapeutic effects of dihydroartemisinin in multiple stages of colitis-associated colorectal cancer. Theranostics, 11: 6225-6239.
7. Li, Q., Q. Ma, J. Cheng, X. Zhou, W. Pu, X. Zhong and X. Guo, 2021. Dihydroartemisinin as a sensitizing agent in cancer therapies. OncoTargets Ther., 14: 2563-2573.
8. Wang, Z., M. Li, Y. Liu, Z. Qiao, T. Bai, L. Yang and B. Liu, 2021. Dihydroartemisinin triggers ferroptosis in primary liver cancer cells by promoting and unfolded protein response-induced upregulation of CHAC1 expression. Oncol. Rep., Vol. 46. 10.3892/or.2021.8191.
9. Han, W., X. Duan, K. Ni, Y. Li, C. Chan and W. Lin, 2022. Co-delivery of dihydroartemisinin and pyropheophorbide-iron elicits ferroptosis to potentiate cancer immunotherapy. Biomaterials, Vol. 280. 10.1016/j.biomaterials.2021.121315.
10. Wong, K.H., D. Yang, S. Chen, C. He and M. Chen, 2022. Development of nanoscale drug delivery systems of dihydroartemisinin for cancer therapy: A review. Asian J. Pharm. Sci., 17: 475-490.
11. Zheng, J., X. Li, W. Yang and F. Zhang, 2021. Dihydroartemisinin regulates apoptosis, migration, and invasion of ovarian cancer cells via mediating RECK. J. Pharmacol. Sci., 146: 71-81.
12. Liu, J.J., W. Tang, M. Fu, X.Q. Gong and L. Kong *et al*., 2019. Development of R_8 modified epirubicin-dihydroartemisinin liposomes for treatment of non-small-cell lung cancer. Artif. Cells Nanomed. Biotechnol., 47: 1947-1960.
13. Wang, S., H. Wang, W. Liang and Y. Huang, 2012. An injectable hybrid nanoparticle-in-oil-in-water submicron emulsion for improved delivery of poorly soluble drugs. Nanoscale Res. Lett., Vol. 7. 10.1186/1556-276X-7-219.
14. Ren, G., P. Chen, J. Tang, W. Guo and R. Wang *et al*., 2020. *In vivo* and *in vitro* evaluation of dihydroartemisinin prodrug nanocomplexes as a nano-drug delivery system: Characterization, pharmacokinetics and pharmacodynamics. RSC Adv., 10: 17270-17279.
15. Bhujbal, S.V., B. Mitra, U. Jain, Y. Gong and A. Agrawal *et al*., 2021. Pharmaceutical amorphous solid dispersion: A review of manufacturing strategies. Acta Pharm. Sin. B, 11: 2505-2536.
16. Alkholifi, F.K., A. Alam, A.I. Foudah and H.S. Yusufoglu, 2023. Phospholipid-based topical nano-hydrogel of mangiferin: Enhanced topical delivery and improved dermatokinetics. Gels, Vol. 9. 10.3390/gels9030178.
17. Febriyenti, S. Rahmi and A. Halim, 2019. Study of gliclazide solid dispersion systems using PVP K-30 and PEG 6000 by solvent method. J. Pharm. Bioallied Sci., 11: 262-267.
18. Pillay, S., K.R. Steingart, G.R. Davies, M. Chaplin and M. de Vos *et al*., 2022. Xpert MTB/XDR for detection of pulmonary tuberculosis and resistance to isoniazid, fluoroquinolones, ethionamide, and amikacin. Cochrane Database Syst. Rev., Vol. 2022. 10.1002/14651858.CD014841.pub2.
19. Akram, J., A.S. Khan, H.A. Khan, S.A. Gilani, S.J. Akram, F.J. Ahmad and R. Mehboob, 2020. Extensively drug-resistant (XDR) typhoid: Evolution, prevention, and its management. BioMed Res. Int., Vol. 2020. 10.1155/2020/6432580.
20. Bouzakher-Ghomrasni, N., O. Taché, J. Leroy, N. Feltin, F. Testard and C. Chivas-Joly, 2021. Dimensional measurement of TiO_2 (nano) particles by SAXS and SEM in powder form. Talanta, Vol. 234. 10.1016/j.talanta.2021.122619.
21. Stoian, A.B., I. Demetrescu and D. Ionita, 2020. Nanotubes and nano pores with chitosan construct on TiZr serving as drug reservoir. Colloids Surf. B: Biointerfaces, Vol. 185. 10.1016/j.colsurfb.2019.110535.
22. Buchwalder, S., A. Borzì, J.D. Leon, F. Bourgeois and C. Nicolier *et al*., 2022. Thermal analysis of parylene thin films for barrier layer applications. Polymers, Vol. 14. 10.3390/polym14173677.
23. Tiernan, H., B. Byrne and S.G. Kazarian, 2020. ATR-FTIR spectroscopy and spectroscopic imaging for the analysis of biopharmaceuticals. Spectrochim. Acta Part A: Mol. Biomol. Spectrosc., Vol. 241. 10.1016/j.saa.2020.118636.
24. Sala, A., D.J. Anderson, P.M. Brennan, H.J. Butler and J.M. Cameron *et al*., 2020. Biofluid diagnostics by FTIR spectroscopy: A platform technology for cancer detection. Cancer Lett., 477: 122-130.
25. Take, M., T. Takeda, H. Ishikawa, M. Matsumoto, K. Nagano and S. Fukushima, 2020. Area under the blood concentration-time curve (AUC) of ethylbenzene concentration in rats: relationship to inhalation and oral administration route-dose. J. Environ. Sci. Health Part A, 55: 1596-1603.
26. Tanaka, M., M. Kikuchi, S. Takasaki, T. Hirasawa and K. Sigeta *et al*., 2019. Limited sampling strategy for the estimation of mycophenolic acid and its acyl glucuronide metabolite area under the concentration-time curve in Japanese lung transplant recipients. J. Pharm. Pharm. Sci., 22: 407-417.
27. Oda, K., Y. Hashiguchi, T. Kimura, Y. Tsuji and K. Shoji *et al*., 2021. Performance of area under the concentration-time curve estimations of vancomycin with limited sampling by a newly developed web application. Pharm. Res., 38: 637-646.
28. Fournel, L., Z. Wu, N. Stadler, D. Damotte and F. Lococo *et al*., 2019. Cisplatin increases PD-L1 expression and optimizes immune check-point blockade in non-small cell lung cancer. Cancer Lett., 464: 5-14.

29. Xie, H., J. Yao, Y. Wang and B. Ni, 2022. Exosome-transmitted circVMP1 facilitates the progression and cisplatin resistance of non-small cell lung cancer by targeting miR-524-5p-METTL3/SOX2 axis. Drug Delivery, 29: 1257-1271.
30. Cui, Z., H. Wang, S. Li, T. Qin and H. Shi *et al*., 2022. Dihydroartemisinin enhances the inhibitory effect of sorafenib on HepG2 cells by inducing ferroptosis and inhibiting energy metabolism. J. Pharmacol. Sci., 148: 73-85.
31. Tan, X., Y. Song, H. Liu, Q. Zhong and A. Rockenbauer *et al*., 2016. Supramolecular host–guest interaction of trityl-nitroxide biradicals with cyclodextrins: Modulation of spin-spin interaction and redox sensitivity. Org. Biomol. Chem., 14: 1694-1701.
32. Galluzzi, L., L. Senovilla, I. Vitale, J. Michels and I. Martins *et al*., 2012. Molecular mechanisms of cisplatin resistance. Oncogene, 31: 1869-1883.
33. Rosenthal, M.R. and C.L. Ng, 2020. *Plasmodium falciparum* artemisinin resistance: The effect of heme, protein damage, and parasite cell stress response. ACS Infect. Dis., 6: 1599-1614.
34. Morana, O., W. Wood and C.D. Gregory, 2022. The apoptosis paradox in cancer. Int. J. Mol. Sci., Vol. 23. 10.3390/ijms23031328.
35. Rana, N.K., P. Singh and B. Koch, 2019. $CoCl_2$ simulated hypoxia induce cell proliferation and alter the expression pattern of hypoxia associated genes involved in angiogenesis and apoptosis. Biol. Res., Vol. 52. 10.1186/s40659-019-0221-z.
36. Shao, C., Y. Liu, Z. Chen, Y. Qin and X. Wang *et al*., 2022. 3D two-photon brain imaging reveals dihydroartemisinin exerts antiepileptic effects by modulating iron homeostasis. Cell Chem. Biol., 29: 43-56.E12.
37. Moss, S., E. Mańko, S. Krishna, S. Campino, T.G. Clark and A. Last, 2022. How has mass drug administration with dihydroartemisinin-piperaquine impacted molecular markers of drug resistance? A systematic review. Malar. J., Vol. 21. 10.1186/s12936-022-04181-y.
38. Mei, J., G. Liu, R. Li, P. Xiao, D. Yang, H. Bai and Y. Hao, 2021. LncRNA SNHG6 knockdown inhibits cisplatin resistance and progression of gastric cancer through miR-1297/BCL-2 axis. Biosci. Rep., Vol. 41. 10.1042/BSR20211885.
39. Tang, T., Q. Xia and M. Xi, 2021. Dihydroartemisinin and its anticancer activity against endometrial carcinoma and cervical cancer: Involvement of apoptosis, autophagy and transferrin receptor. Singapore Med. J., 62: 96-103.
40. Changizi, Z., A. Moslehi, A.H. Rohani and A. Eidi, 2021. Chlorogenic acid induces 4T1 breast cancer tumor's apoptosis via p53, Bax, Bcl-2, and caspase-3 signaling pathways in BALB/c mice. J. Biochem. Mol. Toxicol., Vol. 35. 10.1002/jbt.22642.
41. Malami, I., A.M. Bunza, A.M. Alhassan, A. Muhammad and I.B. Abubakar *et al*., 2022. Dihydroartemisinin as a potential drug candidate for cancer therapy: A structural-based virtual screening for multitarget profiling. J. Biomol. Struct. Dyn., 40: 1347-1362.
42. Iksen, S. Pothongsrisit and V. Pongrakhananon, 2021. Targeting the PI3K/AKT/mTOR signaling pathway in lung cancer: An update regarding potential drugs and natural products. Molecules, Vol. 26. 10.3390/molecules26134100.
43. Lin, Y., L. Zhang, X. Ding, C. Chen, M. Meng, Y. Ke and W. Wang, 2022. Relationship between the microRNAs and PI3K/AKT/mTOR axis: Focus on non-small cell lung cancer. Pathol. Res. Pract., Vol. 239. 10.1016/j.prp.2022.154093.
44. Ba, Q., J. Duan, J.Q. Tian, Z.L. Wang and T. Chen *et al*., 2013. Dihydroartemisinin promotes angiogenesis during the early embryonic development of zebrafish. Acta Pharmacol. Sin., 34: 1101-1107.
45. Liang, R., W. Chen, X.Y. Chen, H.N. Fan, J. Zhang and J.S. Zhu, 2021. Dihydroartemisinin inhibits the tumorigenesis and invasion of gastric cancer by regulating STAT1/KDR/MMP9 and P53/BCL2L1/CASP3/7 pathways. Pathol. Res. Pract., Vol. 218. 10.1016/j.prp.2020.153318.